

Two Dimensional Spin-Polarized Electron Gas at the Oxide Interfaces

B. R. K. Nanda and S. Satpathy

Department of Physics & Astronomy, University of Missouri, Columbia, MO 65211

(Dated: December 1, 2018)

The formation of a novel spin-polarized 2D electron gas at the LaMnO₃ monolayer embedded in SrMnO₃ is predicted from the first-principles density-functional calculations. The La (d) electrons become confined in the direction normal to the interface in the potential well of the La layer, serving as a positively-charged layer of electron donors. These electrons mediate a ferromagnetic alignment of the Mn t_{2g} spins near the interface via the Anderson-Hasegawa double exchange and become, in turn, spin-polarized due to the internal magnetic fields of the Mn moments.

PACS numbers: 75.70.Cn, 73.20.-r, 71.10.Ca, 71.20.-b

Recent advances in the fabrication of high-quality epitaxial interfaces between perovskite oxides have led to a rapid surge of interest in the study of new interface electronic states. A number of oxide interfaces have been shown to possess electrons confined to the interface region forming a two-dimensional electron gas (2DEG). A clear example is an isolated [100] monolayer of LaTiO₃ grown in a SrTiO₃ host^{1,2,3,4}. The trivalent La substituting for the divalent Sr in essence behaves as a positively-charged layer of electron-donor dopants producing a wedge-shaped potential at the interface, where the electrons become confined. A similar type of electron gas has been observed at the much studied LaAlO₃/SrTiO₃ interface⁵, although the exact origin of the electron gas there remains controversial. A somewhat different physics resulting from the interface polarization charges produces the 2DEG at the nitride and the oxide interfaces such as GaN/Al_xGa_{1-x}N⁶ and ZnO/Mg_xZn_{1-x}O⁷. These electron gases often show clear Shubnikov-de Haas oscillations and even superconductivity has been observed in one of the systems just recently.⁸

Since many of these oxides contain magnetic atoms as well, the question arises as to whether one may be able to get a spin-polarized electron gas at the interface, using the internal magnetic fields due to these magnetic atoms. In this Letter, we predict from density-functional band calculations the existence of just such a phase at the manganite interface structure consisting of a LaMnO₃ (LMO) monolayer embedded in the SrMnO₃ (SMO) bulk, sketched in Fig. 1.

The results presented here are obtained from density-functional (DFT) studies of the (LMO)₁/(SMO)₇ layered superlattice using the linear augmented plane wave (LAPW)⁹ and the linear muffin-tin orbitals method (LMTO)¹⁰ with generalized gradient approximation (GGA)¹¹ or the Coulomb-corrected local spin density approximation (LSDA+U) for the exchange-correlation potential. The supercell consisted of twice this formula unit because of the magnetic structures considered in the paper. The structural relaxation was performed using the LAPW-GGA method for the magnetic structure. The calculated cubic lattice constant for the La compound is 3.915 Å and for the Sr compound is 3.802 Å, which are

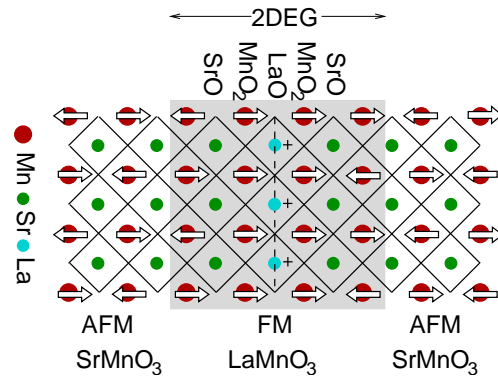


FIG. 1: (color online) The manganite interface structure with a monolayer of LaMnO₃ embedded in the SrMnO₃ bulk, with the shadowed region indicating the spin-polarized 2DEG confined to the interface region. Oxygen atoms occur at the intersections of the checkered lines and form MnO₆ octahedra around the Mn atoms.

close to the experimental values of 3.935 Å and 3.805 Å respectively. For the purpose of relaxation, we fixed the in-plane lattice parameter of the superlattice to be 3.802 Å corresponding to the bulk lattice constant of the Sr compound. This was also the lattice constant for the SMO part in the direction normal to the superlattice, while the same for the LMO monolayer was taken to be 4.15 Å, which conserves the volume of the LMO unit cell in the bulk. The atoms were then relaxed along the c-axis as the symmetry prohibits their motion along the plane.

The results, presented in Fig. 2, indicates the movement of the cations away from the interface, while the anions move towards the interface due to the electrostatic attraction with the positively-charged La layer. This is similar to the cation-anion polarization obtained for the (SrTiO₃)_n/(LaTiO₃)₁ heterostructure, where there also exists at the interface a positively-charged layer of La atoms.^{3,4,12} The electronic structure for the relaxed lattice was obtained using the LMTO method with the LSDA+U approximation, using the Coulomb and the exchange interaction parameters of $U = 5$ eV and $J = 1$ eV.

The magnetic ground states of the two bulk com-

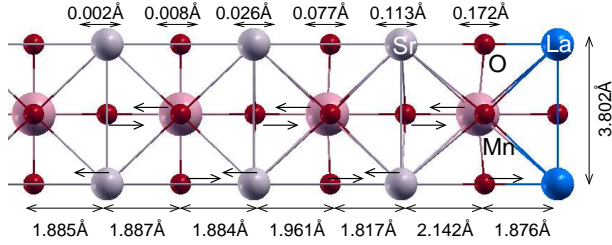


FIG. 2: (color online) Relaxed atomic positions for the $(\text{LMO})_1/(\text{SMO})_7$ superlattice. The atomic displacements, shown by arrows, indicate that the cation-anion polarizations diminish quickly as one goes away from the interface.

pounds are very different. While SMO with its Mn^{4+} ($t_{2g}^3 e_g^0$) configuration is a G-type antiferromagnet (AFM) with the magnetic interaction between the Mn core spins driven by superexchange¹³, LMO is an A-type antiferromagnet with Mn^{3+} ($t_{2g}^3 e_g^1$) electronic configuration, with the partially-filled e_g electrons mediating a ferromagnetic double exchange between the t_{2g} core spins on the MnO_2 planes^{14,15}. For the present interface, there is just one extra electron per La atom, which is localized near the interface, occupying the Mn e_g orbitals (see Fig. 3). These electrons serving as the itinerant electrons in the standard double exchange picture¹⁶ are expected to modify the magnetism of the Mn t_{2g} core spins at the interface.

In order to study the magnetic ground state at the interface, we have considered several magnetic configurations and computed their total energies. We find the lowest-energy structure to be the one shown in Fig. 1, where the two MnO_2 layers on either side of the La layer are ferromagnetic, while the remaining Mn atoms retain the Néel G-type AFM of the SMO bulk. The rest three structures that we examined all have higher energies, viz., (i) the structure with a complete G-type magnetism, (ii) one where the layer ferromagnetism is extended up to the second MnO_2 layer on either side of the interface, and (iii) the structure with the two MnO_2 layers across the interface aligned antiferromagnetically, rather than ferromagnetically as in Fig. 1. The layer ferromagnetic alignment at the interface is explained by the fact that the itinerant e_g electrons mediating the double exchange reside predominantly in the two layers adjacent to the interface, even though a small e_g charge spreads to layers beyond the first layer as seen from Fig. 3.

We note that the magnetic structure of the interface is very much dependent on the strain condition.^{17,18} In the present work, the lattice constant along the interface corresponds to the SMO bulk lattice. For a strong enough tensile or compressive strain, the layer ferromagnetic structure shown in Fig. 1 is no longer energetically favorable;¹⁸ Consequently, the spin-polarized 2DEG will not exist for these strain conditions.

The variation of the potential seen by the electron at the interface may be calculated from the variation of some reference energy in the LMTO calculation. A convenient reference energy is the cell-averaged point-charge

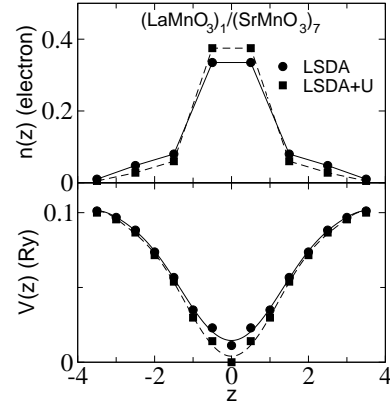


FIG. 3: The cell-averaged potential $V(z)$ calculated from Eq. (1) with distance z from the La layer in units of SrMnO_3 monolayer thickness (bottom), and the donated electrons from La, one per atom, occupying the e_g orbitals of the adjacent Mn atoms (top). The layer occupancy $n(z)$ is the occupancy of electrons for the individual MnO_2 layers and they have predominantly Mn e_g character.

Coulomb potential V , shown in Fig. 3, which was calculated by first averaging the potential over the volume of the i -th Wigner-Seitz atomic sphere:^{2,19}

$$V_i = \frac{3q_i}{2s_i} + \sum_j \frac{q_j}{|r_i - r_j|} \quad (1)$$

and then by averaging over all spheres with a weight factor proportional to their volumes: $V = \sum_i \Omega_i V_i / \sum_i \Omega_i$, where $\Omega_i = 4\pi s_i^3/3$ is the sphere volume, s_i is the sphere radius, r_i its position, and q_i is the total charge, nuclear plus electronic. In Eq. (1), the first term is the sphere average of the potential of the point charge located at the center of the muffin-tin sphere and the second term is the Madelung potential due to all other spheres in the solid.

The results plotted in Fig. 3 shows the screening of the bare linear potential due to the electrostatic field of the charged La plane caused by the electronic as well as the lattice polarization. The screened potential is deep enough to localize the donor electron within just a few layers of the interface. In fact, we find that about $0.7 e^-$ is located on the first MnO_2 layers, $0.14 e^-$ on the second layers, and the remaining $0.16 e^-$ is spread between the remaining atoms.

The presence of a substantial amount of the e_g charge on the first MnO_2 layer is consistent with the double exchange mechanism for the layer ferromagnetism (Fig. 1) found from the DFT calculations. However, although in the DFT results, the structure, where the second MnO_2 layer is also ferromagnetic in addition to the first, was not energetically favorable, the leaked e_g electrons into the second layer could result in a canted ferromagnetic state for this layer. Whether a canted state forms or the antiferromagnetism is retained depends on the amount of charge leakage into this layer and the strength of the

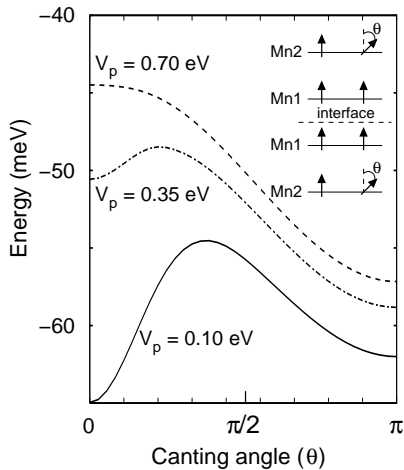


FIG. 4: Total energy obtained from Eq. 2 as a function of the canting angle between the nearest neighbor Mn spins in the second MnO₂ layer for different values of the potential V_p . A magnitude of $V_p \approx 0.5$ eV, which results in roughly the same electron leakage into the second layer as obtained from the DFT, yields an antiferromagnetic ground state as inferred from the figure, indicating the absence of a canted state.

double exchange interaction.

To address this issue, we have studied the Anderson-Hasegawa double-exchange model¹⁶ on a four-layer lattice (Fig. 4, inset), each layer being a square lattice, as appropriate for the MnO₂ layers. The model Hamiltonian, restricted to the Mn sites up to second MnO₂ planes away from the interface, is given by

$$H = \sum_{i\sigma} \epsilon_{i\sigma} n_{i\sigma} + t \sum_{\langle ij \rangle \sigma} c_{i\sigma}^\dagger c_{j\sigma} + H.c. + J \sum_{\langle ij \rangle} \vec{S}_i \cdot \vec{S}_j - 2J_H \sum_i \vec{S}_i \cdot \vec{s}_i, \quad (2)$$

and it describes the double exchange interaction of the itinerant electrons in a lattice of localized spins. Here, $c_{i\sigma}^\dagger$, $c_{i\sigma}$ are the field operators for the e_g carriers, treated within a one-band model, with i, σ being the site and spin indices, \vec{S}_i is the localized t_{2g} spin and $\vec{s}_i = \frac{1}{2} \sum_{\mu\nu} c_{i\mu}^\dagger \vec{\tau}_{\mu\nu} c_{i\nu}$ is the itinerant spin electron density, with $\vec{\tau}$ being the Pauli spin matrices. The onsite energy $\epsilon_{i\sigma}$ (V_p on the second layer and zero on the first) describes the electric field at the interface and is the parameter that controls the leakage of the itinerant electron into the second layer. J is the superexchange interaction between the localized spins, while J_H is the Hund's coupling between the itinerant and the localized electrons. Guided by the earlier DFT calculations^{14,20,21} the typical values of the parameters are: $t \sim -0.15$ eV, $J \sim 7$ meV, and $J_H \sim 1$ eV. Note that unlike our earlier work,²² here we neglect the on-site Coulomb energy between the itinerant carriers, since the number of carriers is small.

The Hamiltonian (2) is solved by diagonalizing a 16×16

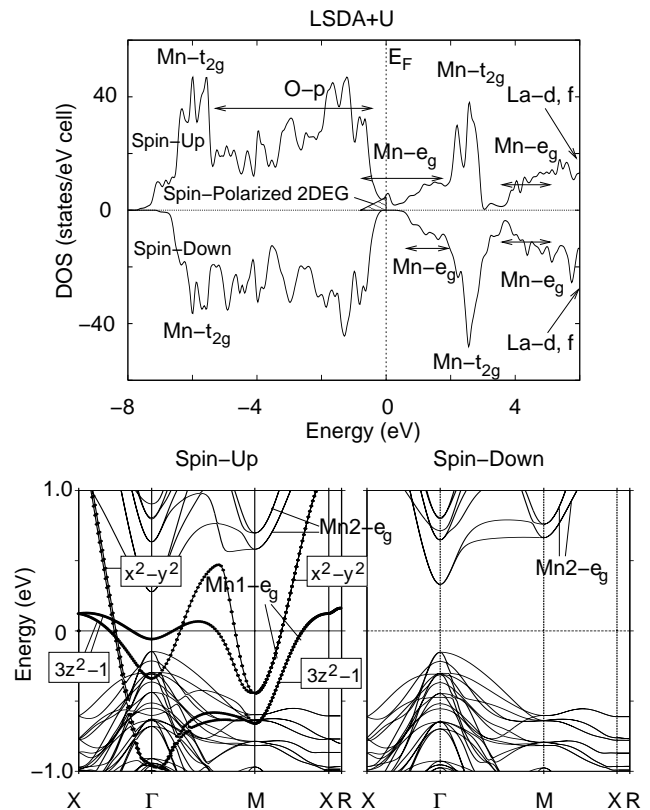


FIG. 5: Total densities of states for the (LMO)₁/(SMO)₇ interface for the majority and the minority spins (top) and the band structure in the vicinity of the Fermi energy (bottom). The symmetry points are: Γ (0, 0, 0), X (1, -1, 0), M (0, 2, 0) and R (1, -1, -2a/c) in units of $\pi/2a$, a being the lattice constant along the plane of the interface. The symbols Mn1 and Mn2 indicate the first and the second layer atoms next to the interface.

Hamiltonian matrix (eight Mn atoms per unit cell and two spin types) for a number of \vec{k} points in the two-dimensional Brillouin zone and the total energy is calculated by summing over the occupied states (two electrons per cell). The results summarized in Fig. 4 show that an antiferromagnetic second layer (canting angle $\theta = \pi$) is overwhelmingly favored over a canted state for a parameter of $V_p \approx 0.5$ eV, which yields roughly the same amount of electron leakage into the second MnO₂ layer as obtained from the DFT calculations.

The electronic structure corresponding to the lowest-energy magnetic structure (Fig. 1) is shown in Fig. 5. The t_{2g} states of one spin are occupied for each Mn atom and lie far below the Fermi energy E_F because of the octahedral crystal field produced by the MnO₆ octahedron and the strong Coulomb repulsion U . The vicinity of E_F is occupied by the Mn- e_g states. In the spin-majority channel, we see extended e_g states crossing the Fermi level, while in the spin-minority channel, they are unoccupied and open up a gap at the Fermi energy, so that we have a half-metallic system.

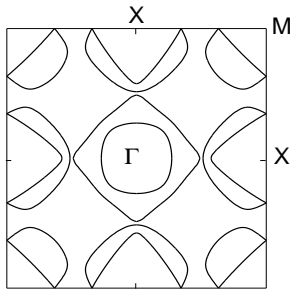


FIG. 6: The Fermi surface of $(\text{LMO})_1/(\text{SMO})_7$ shown in the interface Brillouin zone.

While there are a number of half metallic systems known, the classic one being Fe_3O_4 ²³, the present case is quite unique in the sense that the electrons at the Fermi energy are confined to the interface region, producing a spin-polarized 2DEG. This is in fact a key point of the paper.

The bands crossing the Fermi energy are the majority-spin $\text{Mn1-}e_g$ (x^2-y^2 and $3z^2-1$) states belonging to the first-layer manganese atoms with bonding interaction across the interface. The corresponding anti-bonding states as well as all minority-spin $\text{Mn1-}e_g$ states occur higher in energy and outside the energy range of Fig. 5. In contrast to this, since the second layer manganese moments are antiferromagnetically organized, the $\text{Mn2-}e_g$ states occur both in the minority and majority spin channels as seen from the figure.

As discussed earlier, the partially occupied e_g states mediate a ferromagnetic double exchange interaction between the t_{2g} core spins, which competes with the antiferromagnetic superexchange. This double exchange interaction is directional in nature in the sense that its strength in the xy -plane or along the z -axis depends on the occupancy of the individual e_g orbitals (x^2-y^2 and $3z^2-1$)^{17,18}. Since we have both orbitals significantly oc-

cupied, this leads to a strong double exchange both in the first MnO_2 layers and between these layers across the interface, resulting in the layer ferromagnetic structure as shown in Fig. 1.

The interface Fermi surface, shown in Fig. 6, is constituted out of the $\text{Mn1-}e_g$ (x^2-y^2 and $3z^2-1$) states and their orbital characters may be inferred from the band structure shown in Fig. 5. The Fermi surface consists of electron-like pockets at the Γ and M points and hole-like pockets centered at the X points. The holes have relatively higher mass, so that the transport along the interface may be expected to be electron like.

Although the interface suggested in this paper has not been grown to our knowledge (but is certainly possible to grow), it is encouraging that there are several experimental works on the LMO/SMO superlattices, which seem to support the existence of a ferromagnetic state at the interface.^{17,24,25} It would be gratifying if the spin-polarized 2DEG can be established experimentally in these oxide systems.

In summary, from density-functional studies, we have predicted the formation of a spin-polarized 2DEG at the LaMnO_3 layer embedded in a thick SrMnO_3 bulk. This occurs due to the confinement of the La electrons near the interface because of the electrostatic potential of the positively-charged La layer. These electrons occupy the $\text{Mn-}e_g$ states near the interface, mediating a double exchange interaction to stabilize a layer ferromagnetic structure of the Mn spins and become, in turn, completely spin-polarized due to the magnetic fields of the Mn atoms. The Néel G-type antiferromagnetism of the bulk SrMnO_3 is retained in the second MnO_2 layer from the interface and beyond. The complete spin-polarization of the electron gas without any external magnetic field is a new feature for the perovskite oxide interfaces.

We acknowledge support of this work by the U. S. Department of Energy through Grant No. DE-FG02-00ER45818.

¹ A. Ohtomo, D. A. Muller, J. L. Grazul, and H. Y. Hwang, *Nature* **419**, 378 (2002)
² Z. S. Popovic and S. Satpathy, *Phys. Rev. Lett.* **94**, 176805 (2005)
³ D. R. Hamann, D. A. Muller, and H. Y. Hwang, *Phys. Rev. B* **73**, 195403 (2006)
⁴ S. Okamoto, A. J. Millis, and N. A. Spaldin, *Phys. Rev. Lett.* **97**, 056802 (2006)
⁵ M. Hujiben *et al.*, *Nature Mat.* **5**, 556 (2006); A. Ohtomo and H. Y. Hwang, *Nature* **427**, 423 (2004)
⁶ D. R. Hang, C. F. Huang, and Y. F. Chen, *Appl. Phys. Lett.* **89**, 092116 (2006)
⁷ A. Tsukazaki, A. Ohtomo, T. Kita, Y. Ohno, and M. Kawasaki, *Science* **315**, 1388 (2007)
⁸ N. Reyren *et al.*, *Science* **317**, 1196 (2007)
⁹ P. Blaha *et al.*, WIEN2k, "An Augmented Plane Wave

+ Local Orbitals Program for Calculating Crystal Properties" (Karlheinz Schwarz, Techn. Universitat Wien, Austria, 2001) ISBN 3-9501031-1-2
¹⁰ O. K. Andersen and O. Jepsen, *Phys. Rev. Lett.* **53**, 2571 (1984)
¹¹ J. P. Perdew and Y. Wang, *Phys. Rev. B* **45**, 13244 (1992); J. P. Perdew, K. Burke, and M. Ernzerhof, *Phys. Rev. Lett.* **77**, 3865 (1996)
¹² P. Larson, Z. Popovic, and S. Satpathy, *Phys. Rev. B* (in press)
¹³ A. J. Millis, *Phys. Rev. B* **55**, 6405 (1997)
¹⁴ S. Satpathy, Z. S. Popovic, and F. R. Vukajlovic, *Phys. Rev. Lett.* **76**, 960 (1996)
¹⁵ D. Feinberg, P. Germain, M. Grilli, and G. Seibold, *Phys. Rev. B* **57**, R5583 (1998)
¹⁶ P. W. Andersen and H. Hasegawa, *Phys. Rev.* **100**, 675

- (1955); C. Zener, Phys. Rev. **82**, 403 (1951); P. -G. de Gennes, Phys. Rev. **118**, 141 (1960)
- ¹⁷ H. Yamada, M. Kawasaki, T. Lottermoser, T. Arima, and Y. Tokura, Appl. Phys. Lett. **89**, 052506 (2006)
- ¹⁸ B. R. K. Nanda and S. Satpathy, to be published.
- ¹⁹ W. R. L. Lambrecht, B. Segall, and O. K. Andersen, Phys. Rev. B **41**, 2813 (1990)
- ²⁰ W. E. Pickett and D. J. Singh, Phys. Rev. B **53**, 1146 (1996)
- ²¹ H. Meskine, H. Konig, and S. Satpathy, Phys. Rev. B **64**, 094433 (2001)
- ²² S. K. Mishra, S. Satpathy, F. Aryasetiawan, and O. Gunnarsson, Phys. Rev. B **55**, 2725 (1997)
- ²³ Z. Zhang and S. Satpathy, Phys. Rev. B **44**, 13319 (1991)
- ²⁴ S. J. May *et al.*, arXiv:0709.1715v2 [cond-mat.mtrl-sci]
- ²⁵ Ş. Smadici *et al.*, Phys. Rev. Lett. **99**, 196404 (2007)